ACS OMEGA

Article

Cite This: ACS Omega 2018, 3, 9790−9797

http://pubs.acs.org/journal/acsodf

Bimetallic Zeolitic Imidazolate Framework as an Intrinsic Two-Photon Fluorescence and pH-Responsive MR Imaging Agent

Gaozheng Zhao,[†] Huihui Wu,[‡] Ruilu Feng,[†] Dongdong Wang,[†] Pengping Xu,[†] Haibao Wang,*[,§] Zhen Guo,*[,‡] and Qianwang Chen*[,†]

[†]Hefei National Laboratory for Physical Sciences at Microscale, Department of Materials Science & Engineering & Collaborative Innovation Center of Suzhou Nano Science and Technology, CAS High Magnetic Field Laboratory, University of Science and Technology of China, Hefei 230026, China

[‡]Anhui Key Laboratory for Cellular Dynamics and Chemical Biology, School of Life Sciences, University of Science and Technology of China, Hefei 230027, China

[§]Radiology Department of the First Affiliated Hospital of Anhui Medical University, Hefei 230022, China

Supporting Information

ABSTRACT: Zeolitic imidazolate framework-8 (ZIF-8) has received wide attention in recent years as a potential drug vehicle for the treatment of cancer due to its acid-responsiveness and moderate biocompatibility. However, its congenital deficiency of intrinsic imaging capability limits its wider applications; therefore, a postsynthetic exchange approach was utilized to introduce paramagnetic manganese-(II) ions into the ZIF-8 matrix. As a result, bimetallic zeolitic imidazolate frameworks (Mn−Zn−ZIF) were thus fabricated and exhibited pH-responsive T1-weighted magnetic resonance imaging (MRI) contrast effect. Remarkably, we also found its own fluorescence derived from 2-methylimidazole, which is the first report of the intrinsic two-photon fluorescence imaging of ZIFs to our knowledge. Mn−Zn−ZIF still preserves the original properties of ZIF-8 of high surface areas, microporosity, and acid sensitivity. After further PEGylation of Mn−Zn−ZIF, the nanoparticles showed no obvious toxicity and its MRI contrast effect has also been enhanced. Our work highlights the promise of modified zeolitic imidazolate frameworks as potential cancer theranostic platforms.

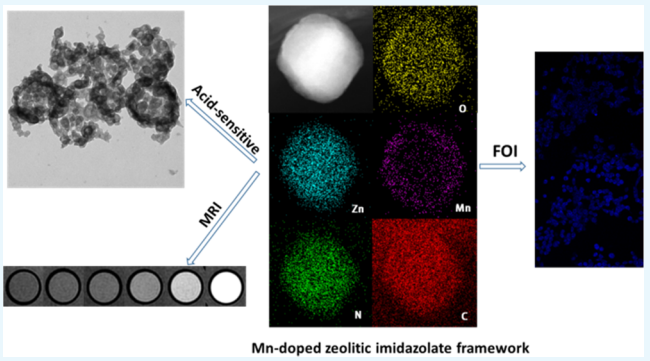

INTRODUCTION

Cancer has posed deadly threats to the health of human beings, causing millions of deaths annually. Among several patterns of curing cancer developed so far, chemotherapy is still the main curing method after surgery due to the high efficacy in reducing tumor size and eliminating tumor residues.[1−5] Over the past few decades, the rapid development of nanotechnology has helped revolutionize traditional chemotherapy. Nanosized vehicles including liposomes,[6] micelles,[7] dendrimers,[8] and inorganic materials[9] are broadly used as drug delivery systems (DDS) to figure out a series of problems[10−13] originating from free drugs, such as unfavorable side effects for healthy cells, poor water solubility, and rapid blood clearance of drugs. However, these conventional nanocarriers have their own limitations in biomedicine; for example, liposomes, micelles, and dendrimers usually have the disadvantage of low loading capacities, and inorganic porous materials usually suffer from poor degradability and unacceptable toxicity.[14] Very recently, metal−organic frameworks (MOFs) composed of various organic linkers and metal joints have emerged as charming delivery vehicles.[14−17] Predominance of exceptionally high surface areas, tunable pore sizes, potential biodegradability, and facilely tailorable functionalities impart them superiority and prospects for applications in delivering therapeutic agents. In particular, a subclass of MOFs, zeolitic imidazolate framework-8 (ZIF-8), built from zinc ions and 2-methylimidazolate, has drawn great attention with stimuli-responsive drug-controlled release for cancer therapy;[18−21] its acid-sensitivity together with moderate biocompatibility endow the DDS with reduced systemic toxicity and enhanced anticancer efficacy in vivo.

On the other hand, an ever-growing demand for efficient therapeutic strategies also requires incorporation of imaging modalities to realize better therapeutic planning and monitoring of therapeutic responses.[22] Theranostics, which integrate cancer therapy and cancer diagnosis, have been a research hotspot for decades,[23−26] and the dual applications of MOFs as drug carriers and potential imaging agents have been

Received: May 7, 2018
Accepted: August 8, 2018
Published: August 23, 2018

DOI: 10.1021/acsomega.8b00923
ACS Omega 2018, 3, 9790−9797

widely reported,[27−29] such as serving as contrast agents (CA) for magnetic resonance (MR) image enhancement[30] and two-photon fluorescence (TPF) imaging probes.[22] However, limited by the properties of central zinc ions, ZIF-8 does not possess MR imaging capability, and other intrinsic diagnosis imaging abilities are also never reported to our knowledge. Usually, the common idea is to combine ZIF-8 with other imaging agents in the form of composites to attain multifunctionality;[18,20,31,32] although this way has been demonstrated effective, it still had some drawbacks such as complicated synthesis steps and reduced drug carrier percentage. It would be encouraging to endow ZIF-8 with imaging abilities while keeping its own crucial properties unchanged. Therefore, these results above inspired us to make modification to ZIF-8 itself to realize a diagnostic platform.

Herein, for incorporating MR imaging ability, a postsynthetic exchange (PSE) approach was utilized to introduce paramagnetic manganese(II) ions into ZIF-8;[33] nanosized manganese-doped zeolitic imidazolate frameworks (denoted as Mn−Zn−ZIF) were thus fabricated. After doping manganese(II) ions into the matrix, Mn−Zn−ZIF still maintains the original pH-responsiveness and exhibits T1-weighted MRI contrast effect. The Brunauer−Emmett−Teller (BET) results reveal Mn−Zn−ZIF still has huge surface area for potential drug loading. Interestingly, we found the intrinsic fluorescence optical imaging ability derived from 2-methylimidazolate. As far as we know, it is the first time to report the intrinsic two-photon fluorescence imaging of ZIFs. Therefore, manganese-doped zeolitic imidazolate frameworks could act as intracellular two-photon fluorescence imaging and pH-responsive T1-weighted MRI contrast agents simultaneously.

RESULTS AND DISCUSSION

Incorporating Mn^{2+} into ZIF-8 has some difficulties due to the structural instability of Mn^{2+}−4N tetrahedral geometry;[34] our experiments revealed that direct reaction of Mn^{2+} with 2-methylimidazole in different solvents would result in the formation of complex molecules instead of crystal structure. Satoshi Horike group had synthesized cubic [Mn(2-methylimidazolate)$_2$] (denoted as Mn−ZIF) from [$Mn(BH_4)_2$·3THF]·$NaBH_4$ under an Ar atmosphere.[34] However, highly unstable structure of Mn−ZIF hindered its further application. Recently, Cohen group reported postsynthetic metal ion and ligand exchange in zeolitic imidazolate frameworks,[33] which inspired us to introduce Mn ions into the framework for further biomedical application. ZIF-8 was utilized as the precursor and PSE approach was carried out according to the report[33] with a modified procedure; after incubation with $Mn(acac)_2$ at 60 °C for 2 days, the nanoparticles (NPs) become brown (as illustrated in Figure S2). To get rid of unreacted $Mn(acac)_2$, another several days incubation in pure methanol was carried out, and then Mn−Zn−ZIF was coated by a thin polydopamine (PDA) layer for further PEGylation (denoted as Mn−Zn−ZIF−PEG) to enhance biocompatibility and hydrophilicity of the NPs. As shown in Figure 1: the overall morphology of Mn−Zn−ZIF changed little compared with the precursor (Figure S1). The dynamic light scattering revealed that the mean diameter of the NPs was about 200 nm (Figure S3), which is suitable for biological applications;[18] a thin layer on the surface of the nanoparticles could be observed after PDA coating and PEGylation (Figure S5). Dark-field scanning transmission electron microscopy (STEM) and electron energy loss spectroscopy (EELS) mapping of one

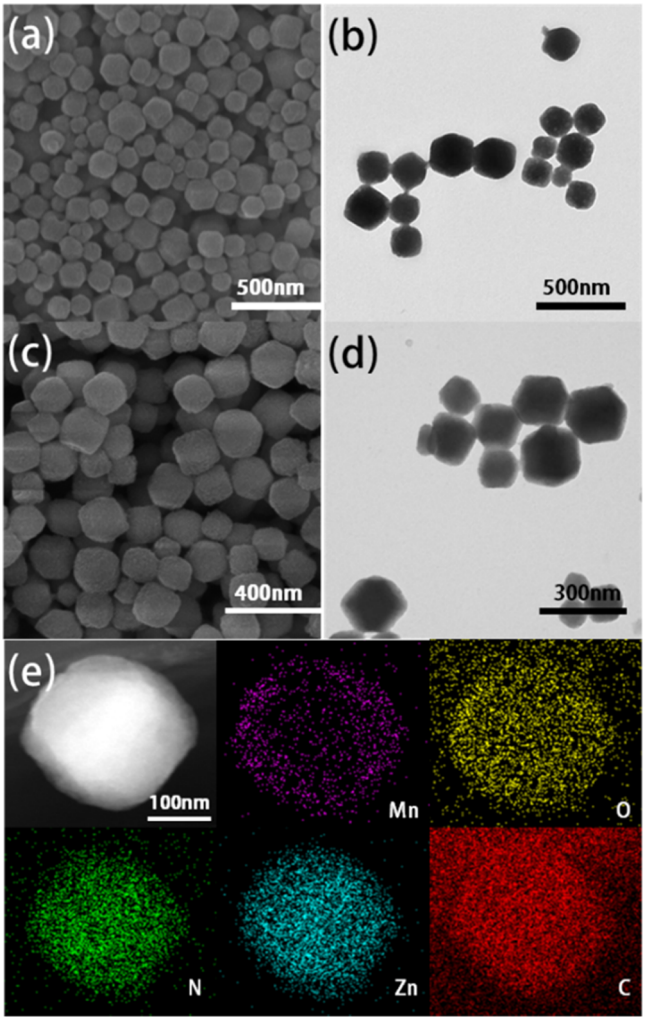

Figure 1. (a) Scanning electron microscopy (SEM) image and (b) telectron microscopy (TEM) image of Mn−Zn−ZIF nanoparticles. (c) SEM image and (d) TEM image of Mn−Zn−ZIF−PEG nanoparticles. (e) Dark-field STEM images and EELS elements mapping of Mn−Zn−ZIF nanoparticles with well-distributed Mn, Zn, C, N, and O elements.

nanoparticle clearly show the spatial distribution of Zn, Mn, N, C, and O elements in the nanoparticle. Obviously, Zn, N, C, and O elements are uniformly distributed and match fairly well with the NP, whereas Mn element displayed inhomogeneous distribution with less amounts existing in the inner core, which revealed the substitution by manganese(II) mainly happening in the exteriors of the NPs.

X-ray diffraction (XRD) pattern of the as-prepared nanoparticles are shown in Figure S4; the peak position of Mn−Zn−ZIF has a good consistency with the standard XRD pattern of ZIF-8, which could verify that the highly porous SOD topology as well as the crystallinity of ZIF-8 was retained after postsynthetic exchange;[33] however, a slight left shift was observed in Mn−Zn−ZIF, as illustrated in Figure 2a, which could verify the successful doping of Mn ions. Fourier transform infrared spectroscopy (FTIR) measurements of $Mn(acac)_2$, ZIF-8, Mn−Zn−ZIF, and Mn−Zn−ZIF−PEG were carried out; as illustrated in Figure 2c, strong characteristic peak of pure $Mn(acac)_2$ such as wavelength at 1557 cm^{-1} was not observed in Mn−Zn−ZIF and Mn−Zn−ZIF−PEG, demonstrating the brown color of the NPs should not simply

DOI: 10.1021/acsomega.8b00923
ACS Omega 2018, 3, 9790−9797

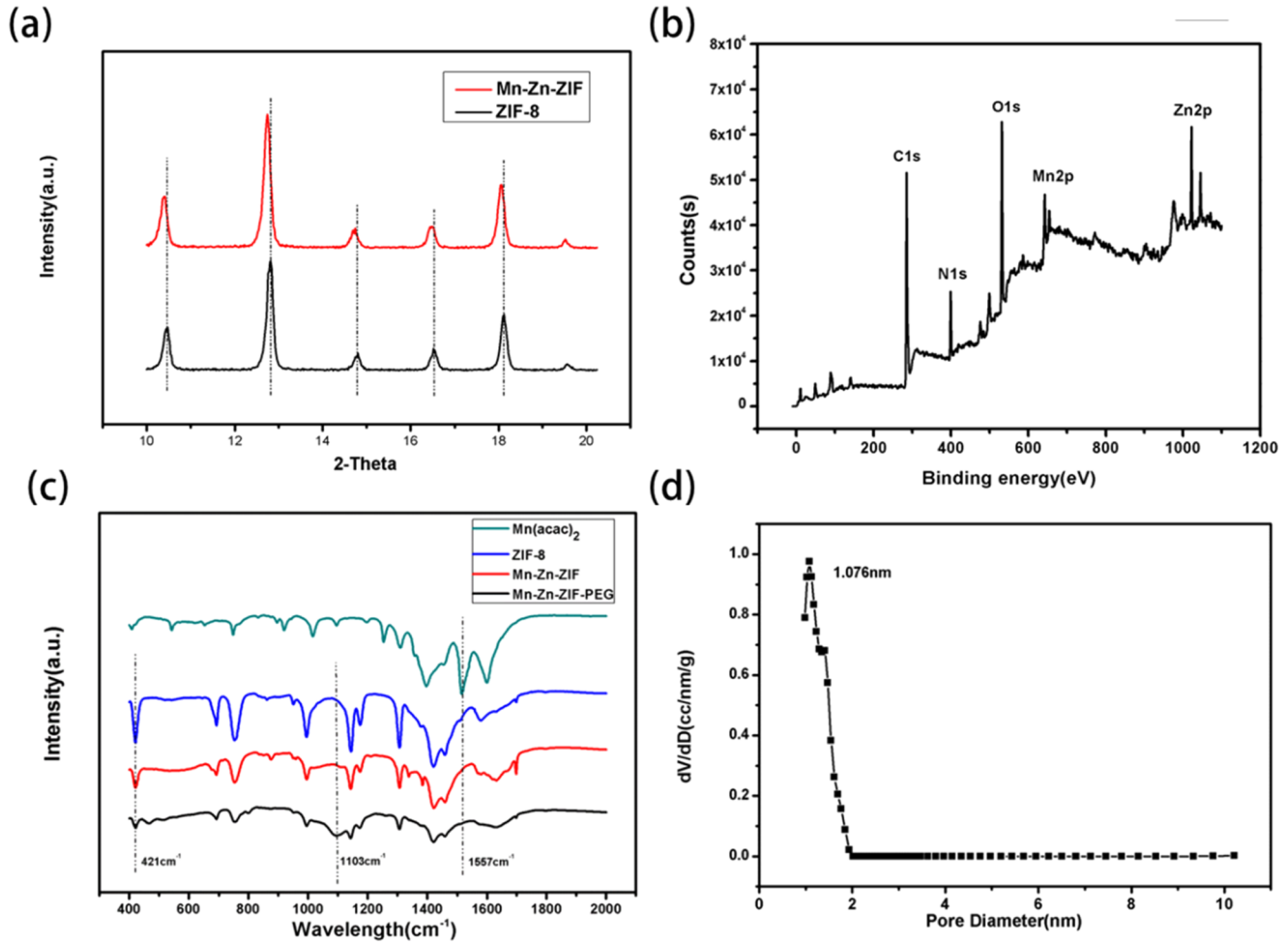

Figure 2. (a) X-ray diffraction (XRD) patterns of synthesized ZIF-8 and Mn−Zn−ZIF nanoparticles from 10 to 20°. (b) X-ray photoelectron spectroscopy pattern of Mn−Zn−ZIF nanoparticles. (c) Fourier transform infrared spectroscopy (FTIR) patterns in the range of 400−2000 cm^{-1} of $Mn(acac)_2$, the precursor ZIF-8, Mn−Zn−ZIF, and Mn−Zn−ZIF−PEG nanoparticles. (d) The corresponding pore size distribution of Mn−Zn−ZIF nanoparticles.

result from the adsorption of $Mn(acac)_2$ by ZIF-8 but doping of Mn ions. The characteristic band of Mn−Zn−ZIF and Mn−Zn−ZIF−PEG at 421 cm^{-1} (Zn−N stretching mode[35]) weakened compared with that of ZIF-8, which could further prove the doping of Mn ions from the side aspect. The appearance of an characteristic band at 1103 cm^{-1} (C−O−C ether stretch band[36]) of Mn−Zn−ZIF−PEG was attributed to CH_2−O−CH_2 group in PEG, revealing the successful PEGylation of Mn−Zn−ZIF. The molar ratio of Mn to Zn was measured to be approximately 1:5.56 ± 0.45 by inductively coupled plasma-atomic emission spectrometry (ICP-AES), indicating around 15% of Zn ions were replaced by Mn ions; as described above, the instability of Mn^{2+}−4N cores restricted the further exchange amount. The presence of Mn in ZIF-8 was also confirmed by X-ray photoelectron spectroscopy (XPS) measurements with the peak at 641.27 eV in spectra. The Brunauer−Emmett−Teller (BET) surface area of Mn−Zn−ZIF NPs was measured to be 1951.01 m^2 g^{-1} with pore size around 1.076 nm, revealing the high specific surface areas and microporosity of Mn−Zn−ZIF for potential drug loading. In conclusion, the above results together with related literature[33,34] convinced the successful fabrication of bimetallic zeolitic imidazolate framework.

After incorporating Mn ions into the matrix, the pH-responsive dissolution property was also examined. Compared with original one, the shape of NPs in phosphate-buffered saline (PBS) solution (pH 5.5) got destroyed, which could be approximately expressed as hollow distribution as shown in Figure 3a,b. The structure was in accordance with the distribution of Mn elements: the doping of manganese was mainly distributed in the exterior of the NPs as shown in the elemental mapping, so it is reasonable to deduce that the coordination between Mn and 2-methylimidazole would be more solid than the coordination between Zn and 2-methylimidazole. At pH 5.5, most of the coordination of Zn and 2-methylimidazole had been destroyed, with quite a part of Mn−2-methylimidazole coordination remaining, forming a hollow structure. The Mn release profile was also measured in PBS solution under pH 5.5 and 7.4; in the first few hours, Mn content had a burst release and gradually went steady and finally 36% of Mn was released at pH 5.5, whereas at pH 7.4, the Mn release had a much lower degradation percentage. The morphology change and the release profile testify the NPs were still sensitive to mild acidity and theoretically could respond to the acidic pH in endosomal/lysosomal compartments of cells.[18] The above results demonstrated that Mn−Zn−ZIF

DOI: 10.1021/acsomega.8b00923
ACS Omega 2018, 3, 9790−9797

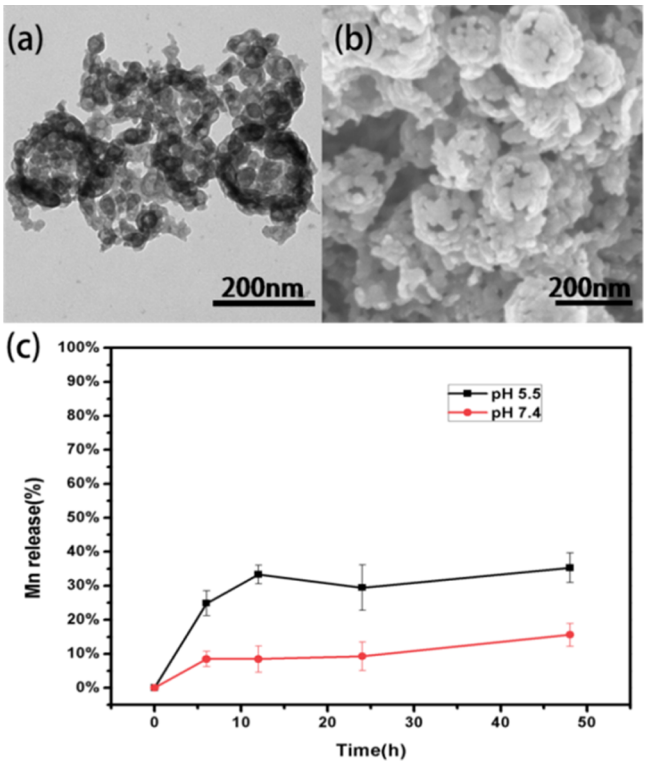

Figure 3. (a) TEM image and (b) SEM image of Mn−Zn−ZIF nanoparticles after immersion in PBS solution (pH 5.5) for 5 min. (c) The percentage of Mn release content over time in PBS solution.

still had decent pH responsiveness after the incorporation, which render it great potentials as a drug delivery carrier.

The NPs (ZIF-8, Mn−Zn−ZIF, and Mn−Zn−ZIF−PEG) were incubated with 4T1 cell lines for 24 h without any further dyeing in a concentration of 100 μg mL^{-1} for fluorescence optical imaging tests by confocal laser scanning microscopy (CLSM). Irradiated by laser beams of 360 nm wavelengths of single-photon excitation (λ_{ex} = 360 nm), the cultured tumor cells emitted blue fluorescence. Fluorescence spectra were examined to figure out the origin of fluorescence, and the emission spectra of 2-methylimidazole, ZIF-8, and Mn−Zn−ZIF were basically consistent with each other upon excitation by 360 nm laser, as illustrated in Figure 4a. The emission peaks were at around 425 nm, which were just located in the blue spectrum region; therefore, we can reasonably infer that the blue fluorescence by 360 nm single-photon excitation was derived from 2-methylimidazole and the fluorescence might be attributed to the $\pi^*-\pi$ transition of 2-methylimidazole according to some literature.[37−39]

However, due to the drawbacks of UV-excited imaging such as undesired tissue photodamage, two-photon fluorescence (TPF) microscopy was thus proposed. With the aids of powerful femtosecond pulse irradiation, the nanoprobes can simultaneously absorb two photons to the excited state and then emit fluorescence after a ground-state relaxation, which is equivalent to half-wavelength excitation of single photon in effect. Two-photon laser scanning microscopy has proved to be an important instrument for directly observing cellular structure and biological process with the superiority of larger penetration depth, less photobleaching and photodamage, and improved resolution compared with traditional confocal microscopy,[40] and adequate absorption cross section of the nanoprobes was required to realize two-photon absorption, so our probe was employed to examine the TPF potentials. Upon biphotonic excitation at 720 nm, ZIF-8, Mn−Zn−ZIF, and Mn−Zn−ZIF−PEG NPs all displayed outstanding fluorescence in the blue spectrum region (Figures 4b,c and S8). Obviously, from the images, fluorescence intensity under 720 nm two-photon excitation was stronger than the one of 360 nm single-photon excitation. As far as we know, it is the first time to report the intrinsic two-photon fluorescence imaging of ZIFs. This two-photon fluorescence imaging potentials of ZIFs provide the feasibility of long-term imaging of cellular process with alleviated photodamage compared to UV-exicited imaging (Figure 5).

MRI measurements were performed by a clinical 3T magnetic resonance scanner. Both Mn−Zn−ZIF and Mn−Zn−ZIF−PEG were respectively dispersed in PBS solution (pH 7.4 and 5.5) with different concentrations to determine

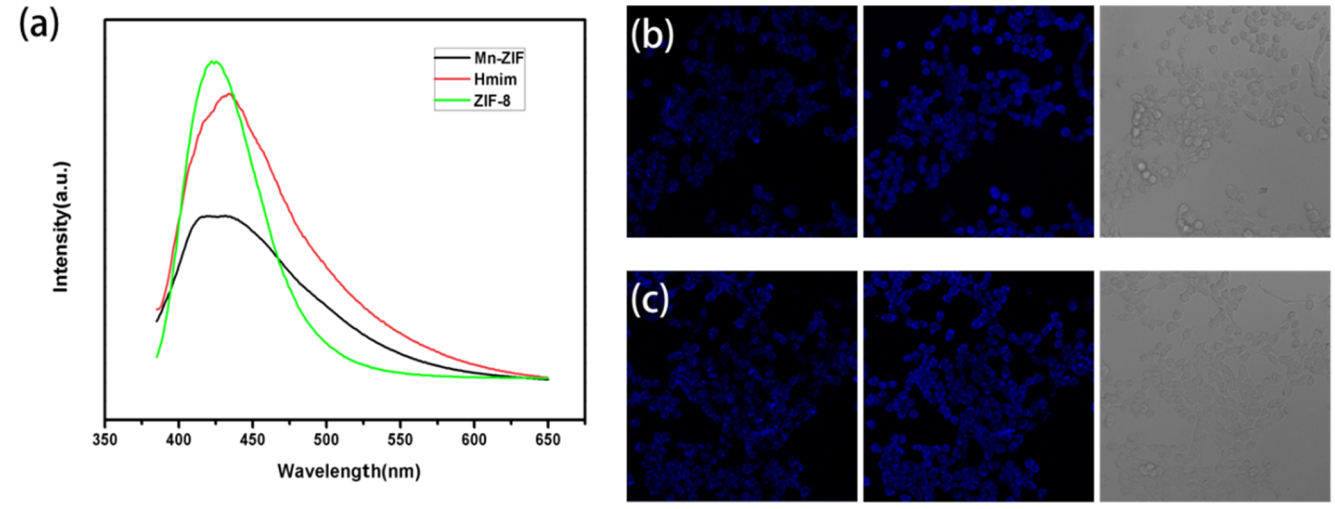

Figure 4. (a) Emission spectra of 2-methylimidazole, ZIF-8, and Mn−Zn−ZIF NPs excited with 360 nm excitation wavelengths (λ_{ex} = 360 nm). (b) CLSM images of Mn−Zn−ZIF incubated with 4T1 cells with different excitation wavelengths (360 nm single-photon excitation, 720 nm two-photon excitation, and bright-field images from left to right). (c) CLSM images of Mn−Zn−ZIF−PEG incubated with 4T1 cells with different excitation wavelengths (360 nm single-photon excitation, 720 nm two-photon excitation, and bright-field images from left to right).

DOI: 10.1021/acsomega.8b00923
ACS Omega 2018, 3, 9790−9797

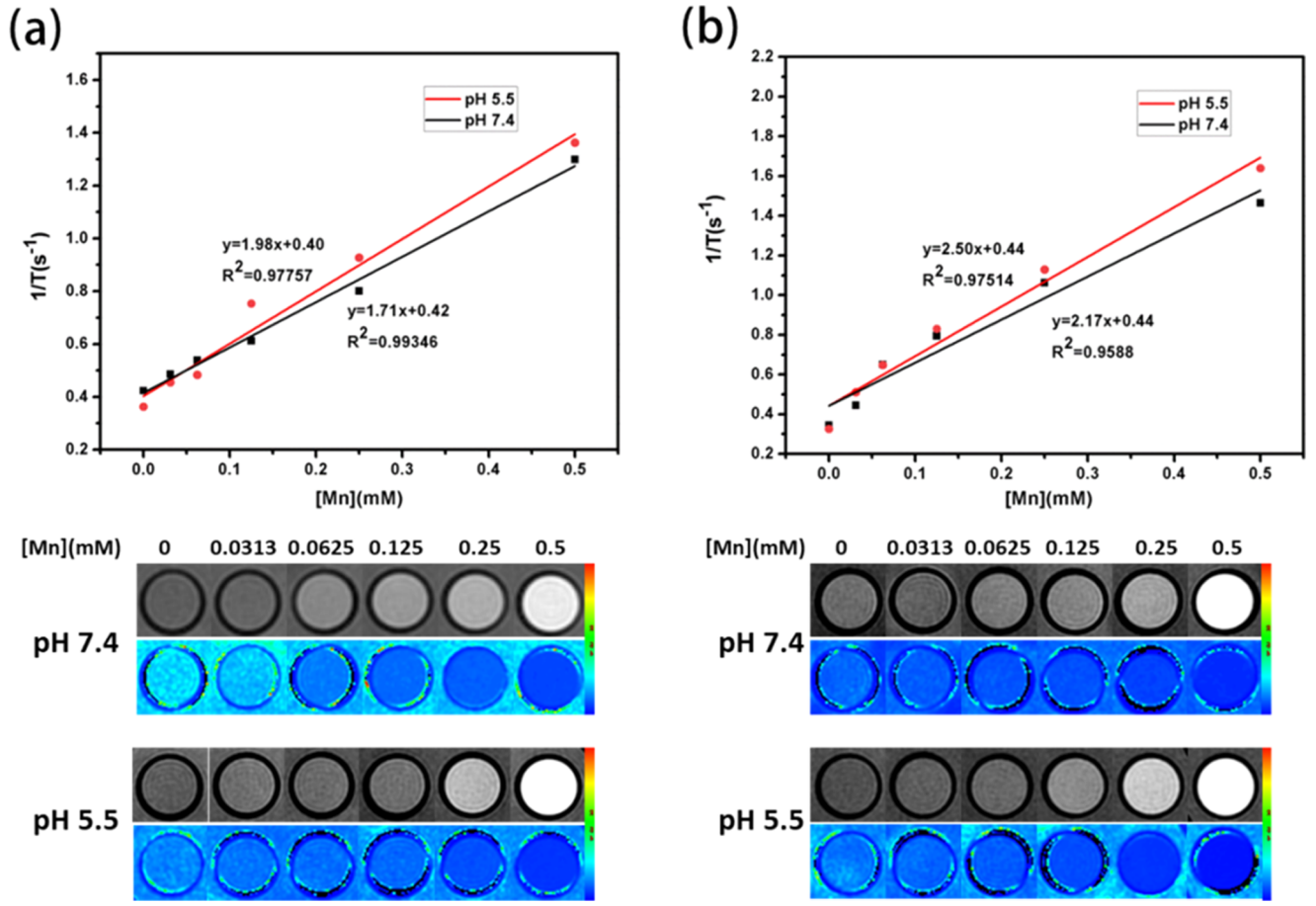

Figure 5. Concentration-dependent relaxation rates over Mn concentration and T1-weighted MR images of (a) Mn−Zn−ZIF nanoparticles and (b) Mn−Zn−ZIF−PEG nanoparticles immersed in PBS solution (pH 7.4, 5.5) for 1 h.

the longitudinal (r_1) relaxivities (Figure 5). The r_1 value of Mn−Zn−ZIF was 1.71 mM s^{-1} at pH 7.4, whereas the value rose to 1.98 mM s^{-1} at pH 5.5. For Mn−Zn−ZIF−PEG NPs, the agent exhibited r_1 value of 2.17 mM s^{-1} at pH 7.4 and the value became 2.50 mM s^{-1} at pH 5.5. The reason for the contrast enhancement at acidic environment was obvious: due to the pH-responsiveness, Mn ions were released from the matrix with decomposition of the NPs, which would enhance the positive contrast effect according to the Solomon−Bloembergen−Morgan theory,[41] and the value change could also prove the acid-sensitivity of Mn−Zn−ZIF in turn. As for the enhancement of Mn−Zn−ZIF−PEG compared to Mn−Zn−ZIF, a similar situation has occurred before:[42] The hydrophilicity of the NPs was enhanced after a thin layer is coated, which contributes to T1 innersphere relaxivity. Although lower than FDA-approved T1 CA (gadolinium-diethylenetriamine penta-acetic acid, r_1 = 4−5 mM^{-1} s^{-1}), the r_1 value of our NPs showed comparable performance to many reported T1 contrast agents.[43−46] The results above indicated the feasibility of the NPs as a T1-weighted contrast agent. Theoretically, the NPs would penetrate the tumor vasculature due to the enhanced permeation and retention effect and accumulate in solid tumors for long periods.[47] The above consequence demonstrated that the NPs offered a multiple-choice platform for biological labels.

MTT assays were carried on 4T1 cell lines to evaluate the cytotoxicity of the Mn−Zn−ZIF and Mn−Zn−ZIF−PEG nanoparticles, Different concentration levels ranging from 12.5 to 75 μg mL^{-1} were assessed. The MTT cell proliferation assay results (Figure 6) demonstrated that Mn−Zn−ZIF nanoparticles showed some toxicity, but the biocompatibility was well enhanced after PEGylation. Obviously, PDA shell and PEGylation not only bring a better MR imaging effect but also make the NPs more biologically biocompatible, and the release of relatively toxic Mn ions could be reduced due to the PDA

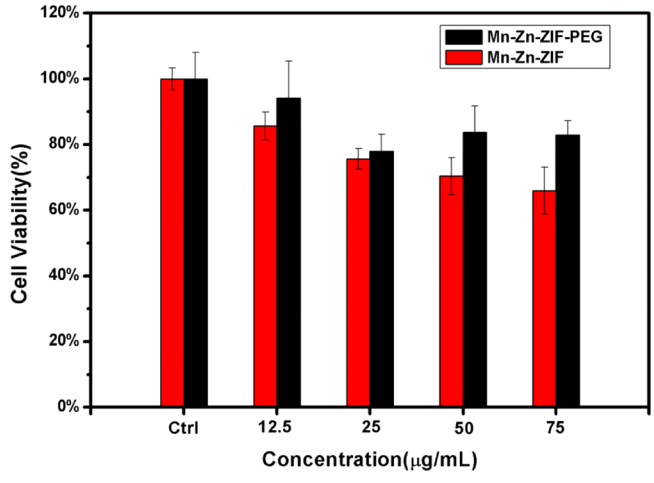

Figure 6. Cell viability of both Mn−Zn−ZIF and Mn−Zn−ZIF−PEG NPs at various concentrations incubated for 24 h.

DOI: 10.1021/acsomega.8b00923
ACS Omega 2018, 3, 9790−9797

coordination.[48] MTT assays show that the sample after decoration has potentials for further in vivo application.

CONCLUSIONS

In summary, manganese-doped zeolitic imidazolate framework was prepared and further PEGylated for the bioimaging application. As expected, Mn−Zn−ZIF and Mn−Zn−ZIF−PEG displayed pH-responsive MR imaging ability; and intrinsic fluorescence of ZIFs can provide the possibility for two-photon fluorescence imaging. The combined imaging modalities derived from the modification or intrinsic property could compensate for the lack of imaging capability of ZIF-8, extending the application of ZIFs to a diagnostic platform. On the other hand, the NPs after modification still preserve the original characteristics of pH-responsiveness, microporosity, and high specific surface areas, rendering it suitable for drug delivery. Although corresponding therapy was not performed, it is reasonable to believe that manganese-doped zeolitic imidazolate framework could serve as a theranostic platform for future application, and further in vivo theranostic experiment would be our next step.

EXPERIMENTAL SECTION

Materials. Poly(vinylpyrrolidone) (K-30) and zinc nitrate hexahydrate ($Zn(NO_3)_2{\cdot}6H_2O$, 99.0%) were purchased from Shanghai Chemical Reagent Company (Shanghai, China); manganese(II) acetyllacetonate (96%) was purchased from Alfa Aesar Company (Shanghai, China); 2-methylimidazole (H-MIM) was purchased from J&K chemical Ltd. (Shanghai, China); dopamine hydrochloride was purchased from Sigma-Aldrich Corporation (Shanghai, China); and methoxy-PEG-*N*-hydroxysuccinimide (mPEG-NHS, MW: 5000) was purchased from Sangon Biotechnology Co., Ltd. (Shanghai, China). All the above chemicals were used without further purification.

Method of Synthesis of Mn−Zn−ZIF. Typically, ZIF-8 was prepared according to the previous report.[49] Then, Mn-doped ZIF-8 was synthesized according to a literature,[33] with a modified procedure: 0.9 g manganese acetyllacetonate was dissolved in 30 mL methanol (MeOH), then 0.3 g ZIF-8 was dispersed in the above solution, and the mixture was incubated at 60 °C in a preheated oven for 48 h. The resulting precipitate (denoted as Mn−Zn−ZIF) was centrifuged and washed several times with MeOH until supernatant become colorless. Then, the nanoparticles were soaked in methanol for 3 days at 60 °C, and the solution was replaced with new MeOH (20 mL) every 24 h. After 3 days of soaking procedure, the precipitate was centrifuged and dried in a vacuum oven.

Method of Synthesis of Mn−Zn−ZIF−PEG. To enhance the biocompatibility and hydrophilicity of Mn−Zn−ZIF, PEGylation of Mn−Zn−ZIF was carried out. Before PEGylation, a thin polydopamine (PDA) layer was coated for easily introducing PEG: 30 mg Mn−Zn−ZIF was dispersed in 8 mL H_2O and then 0.5 mg dopamine hydrochloride was added; due to the resulting alkalinity from a small amount of 2-methylimidazole dissolution, no Tris(hydroxymethyl)-aminomethane (Tris−HCl) was needed. After stirring for 60 min, the precipitate was centrifuged and washed several times with H_2O. Then, the precipitate was redispersed in 8 mL H_2O and then 20 mg mPEG-NHS was added. The solution was stirred for 12 h and then centrifuged and washed several times with H_2O and dried in a vacuum oven.

Characterization. The morphology of the nanostructured material was observed using a field emission scanning electron microscopy (JEOL JSM-6700M) and a transmission electron microscope (TEM, Hitachi H7650). The crystal structure of the material was measured by an X-ray diffractometer (XRD, Rigaku D/MAX-cA, Japan); 2θ scanning range was 10−70°. Metal-ion concentrations were measured with an Optima 7300DV inductively coupled plasma atomic emission spectrometer (ICP-AES). The surface electronic structure was characterized by X-ray photoelectron spectroscopy (XPS, VGESCALAB MKII). High-resolution transmission electron microscopy (STEM, JEM2100F) was used to characterize the distribution of Mn, Zn, O, C, and N elements in the sample. A Magna-IR 750 spectrometer was utilized to obtain the FTIR spectrum in the range of 500−4000 cm^{-1}. Specific surface areas were obtained according to N_2 physisorption results at 77 K (Micromeritics ASAP 2020) by the Brunauer−Emmet−Teller (BET) equation, and density functional theory (DFT) formula was applied to the adsorption branch to acquire the pore size distribution.

Mn Release Measurements. To record the Mn release profile over time, 1 mg Mn−Zn−ZIF was dispersed in PBS solution (pH 5.5 and pH 7.4) and centrifuged at specific time (6, 12, 24, and 48 h) at the speed of 11 000 rpm for 5 min; then, Mn concentrations of the supernatants were characterized by ICP-AES. Three sets of experiments were conducted in every group to get standard error bars.

In Vitro MRI Measurements. Based on the Mn content of Mn−Zn−ZIF and Mn−Zn−ZIF−PEG measured by ICP-AES, different concentrations of Mn−Zn−ZIF and Mn−Zn−ZIF−PEG were dispersed in the PBS solution (pH 5.5 and 7.4) and clinical magnetic resonance scanner (GE Signa HDxt 3.0 Tesla MRI system) was applied to measure the relaxation characteristics. The T1-weighted magnetic resonance imaging images were acquired by utilizing a saturated recovery spin echo sequence (TE = 10 ms, TR = 4000, 2000, 1000, 500, 200, and 100 ms).

In Vitro Fluorescence Microscopy Measurement. The ZIF-8, Mn−Zn−ZIF, and Mn−Zn−ZIF−PEG nanoparticles were cultured with 4T1 cells for 24 h, followed by in vitro laser confocal scanning fluorescence measurements. The detailed procedure can be found in the previous literature[22] and then incubation images were taken with a laser scanning microscope (Zeiss L SM 710) equipped with a 63_1.3 numerical aperture PlanApo objective.

In Vitro Cellular Toxicity Test. Cytotoxicity of the NPs and the PEGylated ones were determined by the tetrazolium dye (MTT) method using 4T1 cell lines. The cells were incubated in a 96-well plate at 37 °C in a moist atmosphere with 100% CO_2 and then the above medium was modified with fetal bovine serum (10%), penicillin (100 units per mL), and streptomycin (100 unit). After culture for 24 h, the solution containing Mn−Zn−ZIF and Mn−Zn−ZIF−PEG nanoparticles were added to replace the original medium. Then, MTT solution was added into each well for another 4 h incubation. Finally, an enzyme-linked immunosorbent assay reader was applied to test the absorbance of each well.

ASSOCIATED CONTENT

Supporting Information

The Supporting Information is available free of charge on the ACS Publications website at DOI: 10.1021/acsomega.8b00923.

DOI: 10.1021/acsomega.8b00923
ACS Omega 2018, 3, 9790−9797

SEM and TEM images of ZIF-8, photograph of ZIFs methanol solution, size distribution of Mn−Zn−ZIF, XRD patterns of ZIFs, FTIR of $Mn(acac)_2$, ZIFs nanoparticles (full spectra), nitrogen adsorption−desorption isotherms curves and the corresponding pore size distribution of ZIFs, CLSM images of ZIF-8 (PDF)

AUTHOR INFORMATION

Corresponding Authors

*E-mail: whblqh@mail.ustc.edu.cn (H.W.).
*E-mail: zhenguo@ustc.edu.cn (Z.G.).
*E-mail: cqw@ustc.edu.cn (Q.C.).

ORCID

Gaozheng Zhao: 0000-0002-6785-4284
Dongdong Wang: 0000-0002-6278-0706

Notes

The authors declare no competing financial interest.

ACKNOWLEDGMENTS

The work was supported by the National Natural Science Foundation of China, 21571168 (Q.C.), The Most Grant 2016YFA0101202 (Z.G.), U1232211 (Q.C.), 31501130 (J.Z.), CAS/SAFEA international partnership program for creative research teams, and CAS Hefei Science Center (2016HSC-IU011).

REFERENCES

(1) Cafeo, G.; Carbotti, G.; Cuzzola, A.; et al. Drug delivery with a calixpyrrole-trans-Pt(II) complex. *J. Am. Chem. Soc.* **2013**, *135*, 2544−2551.
(2) Hubbell, J. A.; Langer, R. Translating materials design to the clinic. *Nat. Mater.* **2013**, *12*, 963−966.
(3) Irvine, D. J. Drug delivery: One nanoparticle, one kill. *Nat. Mater.* **2011**, *10*, 342−343.
(4) Mura, S.; Nicolas, J.; Couvreur, P. Stimuli-responsive nanocarriers for drug delivery. *Nat. Mater.* **2013**, *12*, 991−1003.
(5) Wu, X.; Sun, X. R.; Guo, Z. Q.; et al. In vivo and in situ tracking cancer chemotherapy by highly photostable NIR fluorescent theranostic prodrug. *J. Am. Chem. Soc.* **2014**, *136*, 3579−3588.
(6) Allen, T. M.; Cullis, P. R. Liposomal drug delivery systems: From concept to clinical applications. *Adv. Drug Delivery Rev.* **2013**, *65*, 36−48.
(7) Qiu, L. Y.; Zheng, C.; Jin, Y.; et al. Polymeric micelles as nanocarriers for drug delivery. *Expert Opin. Ther. Pat.* **2007**, *17*, 819−830.
(8) Kesharwani, P.; Jain, K.; Jain, N. K. Dendrimer as nanocarrier for drug delivery. *Prog. Polym. Sci.* **2014**, *39*, 268−307.
(9) Kim, C. S.; Tonga, G. Y.; Solfiell, D.; et al. Inorganic nanosystems for therapeutic delivery: Status and prospects. *Adv. Drug Delivery Rev.* **2013**, *65*, 93−99.
(10) McCarron, P. A.; Marouf, W. M.; Quinn, D. J.; et al. Antibody targeting of camptothecin-loaded PLGA nanoparticles to tumor cells. *Bioconjugate Chem.* **2008**, *19*, 1561−1569.
(11) Min, K. H.; Park, K.; Kim, Y. S.; et al. Hydrophobically modified glycol chitosan nanoparticles-encapsulated camptothecin enhance the drug stability and tumor targeting in cancer therapy. *J. Controlled Release* **2008**, *127*, 208−218.
(12) Nehate, C.; Jain, S.; Saneja, A.; et al. Paclitaxel formulations: Challenges and novel delivery options. *Curr. Drug Delivery* **2014**, *11*, 666−686.
(13) Wang, D.; Zhou, J. J.; Chen, R. H.; et al. Magnetically guided delivery of DHA and Fe ions for enhanced cancer therapy based on pH-responsive degradation of DHA-loaded Fe_3O_4@C@MIL-100(Fe) nanoparticles. *Biomaterials* **2016**, *107*, 88−101.
(14) Wu, M. X.; Yang, Y. W. Metal-organic framework (MOF)-based drug/cargo delivery and cancer therapy. *Adv. Mater.* **2017**, *29*, No. 1605134.
(15) Sun, C. Y.; Qin, C.; Wang, X. L.; et al. Metal-organic frameworks as potential drug delivery systems. *Expert Opin. Drug. Delivery* **2013**, *10*, 89−101.
(16) Wang, D.; Zhou, J. J.; Chen, R. H.; et al. Controllable synthesis of dual-MOFs nanostructures for pH-responsive artemisinin delivery, magnetic resonance and optical dual-model imaging-guided chemo/photothermal combinational cancer therapy. *Biomaterials* **2016**, *100*, 27−40.
(17) Horcajada, P.; Chalati, T.; Serre, C.; et al. Porous metal-organic-framework nanoscale carriers as a potential platform for drug delivery and imaging. *Nat. Mater.* **2010**, *9*, 172−178.
(18) He, M.; Zhou, J. J.; Chen, J.; et al. Fe_3O_4@carbon@zeolitic imidazolate framework-8 nanoparticles as multifunctional pH-responsive drug delivery vehicles for tumor therapy in vivo. *J. Mater. Chem. B* **2015**, *3*, 9033−9042.
(19) Sun, C. Y.; Qin, C.; Wang, X. L.; et al. Zeolitic imidazolate framework-8 as efficient pH-sensitive drug delivery vehicle. *Dalton Trans.* **2012**, *41*, 6906−6909.
(20) Wang, D.; Zhou, J. J.; Shi, R. H.; et al. Biodegradable core-shell dual-metal-organic-frameworks nanotheranostic agent for multiple imaging guided combination cancer therapy. *Theranostics* **2017**, *7*, 4605−4617.
(21) Zhuang, J.; Kuo, C. H.; Chou, L. Y.; et al. Optimized metal-organic-framework nanospheres for drug delivery: Evaluation of small-molecule encapsulation. *ACS Nano* **2014**, *8*, 2812−2819.
(22) Wang, D.; Guo, Z.; Zhou, J. J.; et al. Novel $Mn_3[Co(CN)_6]_2$@SiO_2@Ag core-shell nanocube: enhanced two-photon fluorescence and magnetic resonance dual-modal imaging-guided photothermal and chemo-therapy. *Small* **2015**, *11*, 5956−5967.
(23) Chen, G.; Qju, H. L.; Prasad, P. N.; et al. Upconversion nanoparticles: Design, nanochemistry, and applications in theranostics. *Chem. Rev.* **2014**, *114*, 5161−5214.
(24) Lim, E. K.; Kim, T.; Paik, S.; et al. Nanomaterials for theranostics: Recent advances and future challenges. *Chem. Rev.* **2015**, *115*, 327−394.
(25) Stoddart, A. Theranostics: biogenic delivery. *Nat. Mater.* **2015**, *14*, 13.
(26) Xie, J.; Lee, S.; Chen, X. Y. Nanoparticle-based theranostic agents. *Adv. Drug Delivery Rev.* **2010**, *62*, 1064−1079.
(27) Cai, W.; Chu, C. C.; Liu, G.; et al. Metal-organic framework-based nanomedicine platforms for drug delivery and molecular imaging. *Small* **2015**, *11*, 4806−4822.
(28) Della Rocca, J.; Liu, D. M.; Lin, W. B. Nanoscale metal-organic frameworks for biomedical imaging and drug delivery. *Acc. Chem. Res.* **2011**, *844*, 957−968.
(29) Taylor-Pashow, K. M. L.; Della Rocca, J.; Xie, Z. G.; et al. Postsynthetic modifications of iron-carboxylate nanoscale metal-organic frameworks for imaging and drug delivery. *J. Am. Chem. Soc.* **2009**, *131*, 14261−14263.
(30) Chowdhury, M. A. Metal-organic-frameworks for biomedical applications in drug delivery, and as MRI contrast agents. *J. Biomed. Mater. Res., Part A* **2017**, *105*, 1184−1194.
(31) Liu, R. L.; Yu, P.; Luo, Z. M.; et al. Multicolor fluorescent carbon nanodots@zeolitic imidazolate framework-8 nanoparticles for simultaneous pH-Responsive drug delivery and fluorescence imaging. *J. Controlled Release* **2017**, *259*, E118−E119.
(32) He, L.; Wang, T. T.; An, J. P.; et al. Carbon nanodots@zeolitic imidazolate framework-8 nanoparticles for simultaneous pH-responsive drug delivery and fluorescence imaging. *CrystEngComm* **2014**, *16*, 3259−3263.
(33) Fei, H.; Cahill, J. F.; Prather, K. A.; et al. Tandem postsynthetic metal ion and ligand exchange in zeolitic imidazolate frameworks. *Inorg. Chem.* **2013**, *52*, 4011−4016.
(34) Kadota, K.; Sivaniah, E.; Bureekaew, S.; et al. Synthesis of Manganese ZIF-8 from $[Mn(BH_4)_2 \bullet 3THF] \bullet NaBH_4$. *Inorg. Chem.* **2017**, *56*, 8744−8747.

DOI: 10.1021/acsomega.8b00923
ACS Omega 2018, 3, 9790−9797

(35) Hu, Y.; Kazemian, H.; Rohani, S.; et al. In situ high pressure study of ZIF-8 by FTIR spectroscopy. *Chem. Commun.* **2011**, *47*, 12694−12696.
(36) Khanna, L.; Verma, N. K. PEG/$CaFe_2O_4$ nanocomposite: Structural, morphological, magnetic and thermal analyses. *Phys. B* **2013**, *427*, 68−75.
(37) Bai, H. Y.; Ma, J. F.; Yang, J.; et al. Eight two-dimensional and three-dimensional metal organic frameworks based on a flexible tetrakis(imidazole) ligand: Synthesis, topological structures, and photo luminescent properties. *Cryst. Growth Des.* **2010**, *10*, 1946−1959.
(38) Shi, X.; Zhu, G. S.; Fang, Q. R.; et al. Novel supramolecular frameworks self-assembled from one-dimensional polymeric coordination chains. *Eur. J. Inorg. Chem.* **2004**, 185−191.
(39) Tian, G.; Zhu, G. S.; Fang, Q. R.; et al. Design, synthesis and fluorescence of two-dimensional pillared layers by connecting infinite one-dimensional chains via 4,4′-bipyridine. *J. Mol. Struct.* **2006**, *787*, 45−49.
(40) Aparicio-Ixta, L.; Ramos-Ortiz, G.; Pichardo-Molina, J. L.; et al. Two-photon excited fluorescence of silica nanoparticles loaded with a fluorene-based monomer and its cross-conjugated polymer: their application to cell imaging. *Nanoscale* **2012**, *4*, 7751−7759.
(41) Caravan, P.; Ellison, J. J.; McMurry, T. J.; et al. Gadolinium(III) chelates as MRI contrast agents: Structure, dynamics, and applications. *Chem. Rev.* **1999**, *99*, 2293−2352.
(42) Huang, Y. M.; Hu, L.; Zhang, T. T.; et al. $Mn_3[Co(CN)_6]_2$ @ SiO_2 core-shell nanocubes: Novel bimodal contrast agents for MRI and optical imaging. *Sci. Rep.* **2013**, *3*, No. 2647.
(43) Huang, C. C.; Khu, N. H.; Yeh, C. S. The characteristics of sub 10 nm manganese oxide T1 contrast agents of different nanostructured morphologies. *Biomaterials* **2010**, *31*, 4073−4078.
(44) Huang, J.; Xie, J.; Chen, K.; et al. HSA coated MnO nanoparticles with prominent MRI contrast for tumor imaging. *Chem. Commun.* **2010**, *46*, 6684−6686.
(45) Nakhjavan, B.; Tahir, M. N.; Panthofer, M.; et al. Synthesis, characterization and functionalization of nearly mono-disperse copper ferrite $Cu_xFe_{3-x}O_4$ nanoparticles. *J. Mater. Chem.* **2011**, *21*, 6909−6915.
(46) Evanics, F.; Diamente, P. R.; van Veggel, F. C. J. M.; et al. Water-soluble GdF_3 and GdF_3/LaF_3 nanoparticles-physical characterization and NMR relaxation properties. *Chem. Mater.* **2006**, *18*, 2499−2505.
(47) Davis, M. E.; Chen, Z.; Shin, D. M. Nanoparticle therapeutics: an emerging treatment modality for cancer. *Nat. Rev. Drug Discovery* **2008**, *7*, 771−782.
(48) Xi, J.; Da, L. Y.; Yang, C. S.; et al. Mn^{2+}-coordinated PDA@DOX/PLGA nanoparticles as a smart theranostic agent for synergistic chemo-photothermal tumor therapy. *Int. J. Nanomed.* **2017**, *12*, 3331−3345.
(49) Zheng, F.; Yang, Y.; Chen, Q. W. High lithium anodic performance of highly nitrogen-doped porous carbon prepared from a metal-organic framework. *Nat. Commun.* **2014**, *5*, No. 5261.

DOI: 10.1021/acsomega.8b00923
ACS Omega 2018, 3, 9790−9797